HAL
open science

Testing scenarios on geological models: Local interface insertion in a 2D mesh and its impact on seismic wave simulation

Capucine Legentil, Jeanne Pellerin, Paul Cupillard, Algiane Froehly, Guillaume Caumon

To cite this version:

Capucine Legentil, Jeanne Pellerin, Paul Cupillard, Algiane Froehly, Guillaume Caumon. Testing scenarios on geological models: Local interface insertion in a 2D mesh and its impact on seismic wave simulation. Computers & Geosciences, 2022, 159, pp.105013. 10.1016/j.cageo.2021.105013 . hal-03602649

HAL Id: hal-03602649

https://hal.science/hal-03602649v1

Submitted on 16 Feb 2023

HAL is a multi-disciplinary open access archive for the deposit and dissemination of scientific research documents, whether they are published or not. The documents may come from teaching and research institutions in France or abroad, or from public or private research centers.

L'archive ouverte pluridisciplinaire **HAL**, est destinée au dépôt et à la diffusion de documents scientifiques de niveau recherche, publiés ou non, émanant des établissements d'enseignement et de recherche français ou étrangers, des laboratoires publics ou privés.

Testing scenarios on geological models: local interface insertion in a 2D mesh and its impact on seismic wave simulation

Capucine Legentil[a], Jeanne Pellerin[b], Paul Cupillard[a], Algiane Froehly[c] and Guillaume Caumon[a]

[a] *Université de Lorraine, CNRS, GeoRessources, 54000 Nancy, France*
[b] *TotalEnergies, 91120 Palaiseau, France*
[c] *inria, DGD-I, Avenue de l'Université, BP 1155 64013 Pau cedex, France*

ARTICLE INFO

Keywords:
Triangle meshing
Gas-water contact
Geomodeling
Uncertainties
Inverse problem

ABSTRACT

In this work, we propose a local updating method to test different contact depth scenarios and assess their impact on wave propagation in the subsurface. We propose to locally modify a 2D geological model and run time-dependent elastic simulations. The input model triangulation is conforming to geological structures. The 2D meshed model is locally updated, which means that only the reservoir compartment is modified. Several model geometries are generated by inserting a new interface, in this paper a gas-water contact that is defined by a scalar field. We quantitatively evaluate the impact of the gas-water contact depth on elastic wave propagation. We run the numerical simulations with Hou10ni2D code, which is based on a Discontinuous Galerkin method. The simulation results are compared to a reference depth by computing the L2-norm at a set of seismic receivers. Results show a consistent behavior: we observe a positive correlation between the depth difference and global L2-norm for all receivers. This approach could therefore be integrated into an inversion loop to determine the position of the fluid contact and reduce uncertainties in the reservoir model from a few seismic sensors.

CRediT authorship contribution statement

Capucine Legentil: Conceptualization, Investigation, Methodology, Software, Writing (original draft). **Jeanne Pellerin:** Conceptualization, Methodology, Supervision, Funding Acquisition, Resources, Validation, Writing (reviewing and editing). **Paul Cupillard:** Conceptualization, Supervision, Funding Acquisition, Validation, Writing (reviewing and editing). **Algiane Froehly:** Software. **Guillaume Caumon:** Conceptualization, Methodology, Supervision, Funding Acquisition, Validation, Writing (reviewing and editing).

1. Introduction

Geological models have been used for decades to make forecasts about the behavior of subsurface reservoirs (e.g., Ringrose and Bentley, 2015), seismic hazards (Shaw et al., 2015) or underground waste disposal (e.g., Allen et al., 2018; Mari and Yven, 2014; Mulrooney et al., 2020). These multi-material models can be seen as three dimensional geological maps identifying the geometry of interfaces such as horizons, faults and intrusions. In general, these models are created from the observations at hand (e.g., borehole and seismic reflection data), then meshed and filled with petrophysical properties before solving the relevant physical equations (Ringrose and Bentley, 2015; Wellmann and Caumon, 2018). However, ambiguities and lack of observations often raise uncertainties about the location or even the existence of some interfaces (see Wellmann and Caumon (2018) and references therein). Additionally, temporal evolution at geological time scales or during subsurface engineering projects may involve geometric changes in the

ORCID(s): 0000-0002-2610-7995 (C. Legentil); 0000-0001-8481-7509 (.J. Pellerin); 0000-0001-5201-3696 (.P. Cupillard); 0000-0002-8943-2939 (.A. Froehly); 0000-0002-7828-4600 (.G. Caumon)

geomodel features. Assessing the impact of the uncertainties and/or the temporal changes on the model forecast is a complex computational challenge, which can be partly addressed by deforming an existing mesh to avoid model reconstruction (Abrahamsen, 1993; Tertois and Mallet, 2007). However, remeshing is needed when interfaces are displaced along faults (Caumon et al., 2003), or when new surfaces are introduced in the model (Suter et al., 2017).

However, the repeated updating of a geological model is a difficult task. There are several strategies to edit an interface or add a new one in an unstructured mesh. The most reliable is to rebuild the model from scratch, compute the connectivity of the layers and fault blocks, and generate a new mesh of the whole model (Bidmon et al., 2004). Another strategy is to directly modify the meshed model (Tertois and Mallet, 2007), but the output mesh validity must be guaranteed.

The insertion of a polygonal line in a 2D triangulated surface is an example of such a mesh updating operation. Although it seems simple at first sight, it can be challenging to implement in a robust way because of limited floating point precision. For example, sequential insertion of several tangential lines representing close stratigraphic surfaces or fractures in a fracture corridor may then raise invalid mesh features such as inverted triangles. A good test of robustness is, therefore, to check that results are consistent and stable when inserting the same interface several times. Exact geometric computations (Lévy, 2016; Li et al., 2005; Shewchuk, 1997) do address these issues in combination with constrained remeshing algorithms (e.g., Si, 2015). However, they involve algorithmic complexity and a computational overhead in terms of memory and time, which makes the problem « solved but practically challenging » (Li et al., 2005). Therefore, we consider in this work a subclass of mesh updating problems where the element to insert is represented implicitly by a level-set of a piecewise linear function defined on the mesh. This considerably simplifies the management of geometric accuracy, as the target interface and the mesh to update are represented on the same data structure. This implicit interface representation has been used in geosciences for structural modeling for several years (e.g., Chilès et al., 2004; Houlding, 1994; Mallet, 1988), and it can be applied both on two-dimensional and three-dimensional models.

In the mesh updating examples mentioned above, the modification is often done locally in areas of particular interest (e.g., subdomains where the uncertainty is large, where sensitivity of the model features is important, or areas where new data have been acquired and the model needs to be edited). Therefore, *local* mesh editing approaches, where the vast majority of the mesh is kept intact, are essential for computational efficiency. However, they raise specific challenges to ensure the mesh conformity between the intact and the edited parts (Caumon et al., 2003; Suter et al., 2017).

If the insertion of lines in a 2D triangle mesh may be implemented efficiently, the corresponding 3D problem, i.e., inserting a triangulated surface or discretized lines in a tetrahedral mesh is more difficult. The steps are the same than in 2D: for each element to insert, compute the intersection with the mesh, then insert the intersected elements in the

mesh.

In this paper, we propose a first step to address the above challenges by taking advantage of recent advances of mesh updating libraries developed for shape optimization. Because implementing robust and efficient mesh generation and mesh modification algorithms is extremely challenging, and since open-source implementations are available for triangle and tetrahedral meshes (Dapogny et al., 2014; Geuzaine and Remacle, 2009; Si, 2015), we focus on the integration of one of these libraries in an automatic uncertainty evaluation workflow. Relying on the level-set formulation of the interface to be inserted in the model, we consider the problem of monitoring the evolution of a gas-water contact in a subsurface reservoir using seismic data. We start from an input meshed model conforming to the main geological structures that is locally updated by inserting the fluid contact in the reservoir layer. For simplicity, we keep these structures frozen and we only assume that the contact depth is unknown. Because fluid content directly affects the effective elastic properties of the porous medium, fluid substitution can, in principle, be detected using seismograms as done for instance in time-lapse seismic surveys (e.g., Arts et al., 2003; Landrø et al., 2003). We quantitatively evaluate the impact of contact depth on the simulation results. Under a simple assumption of horizontal fluid contact, we show that our approach can be integrated into an inversion loop to determine the depth of the fluid contact and reduce uncertainties in the reservoir model from only a few seismic sensors.

The contributions of this paper are the following: a practical approach to automatically update triangular meshes for physical simulations is proposed. A special care is taken to the mesh validity, so that the model is suitable for physical simulations. An assessment of the detectability of fluid contacts changes in reservoirs is presented. The algorithms are available on Github and distributed under a GPL license, allowing reproducibility.

The geological models we consider are meshed with triangles that are conforming to geological interfaces such as horizons and faults (Figure 1). We propose to modify a single layer (or region of the model) using the remeshing platform Mmg (Dapogny et al., 2014) (Section 3.2.1). This library, initially developed by Dobrzynski and Frey (2008), has been extended with level-set functionalities and is used to solve shape optimization problems (e.g., Allaire et al., 2004; Osher and Santosa, 2001; Sethian and Wiegmann, 2000). A few adaptations enable to use this library to modify geological models (Section 3.2) and a careful choice of options enables to obtain meshes of good quality, for numerical simulations (Section 4). The approach is demonstrated on a simple synthetic model. Seismic wave propagation simulations are computed using the Discontinuous Galerkin approach implemented in Hou10ni2D [Hu-dee-nee] (Barucq et al., 2014; Barucq, 2016) (Section 4.1). The simulation results for different gas-water contact depth are compared to a reference one in order to solve a Bayesian inverse problem, leading to a probabilistic estimation of the contact depth (Section 4.2).

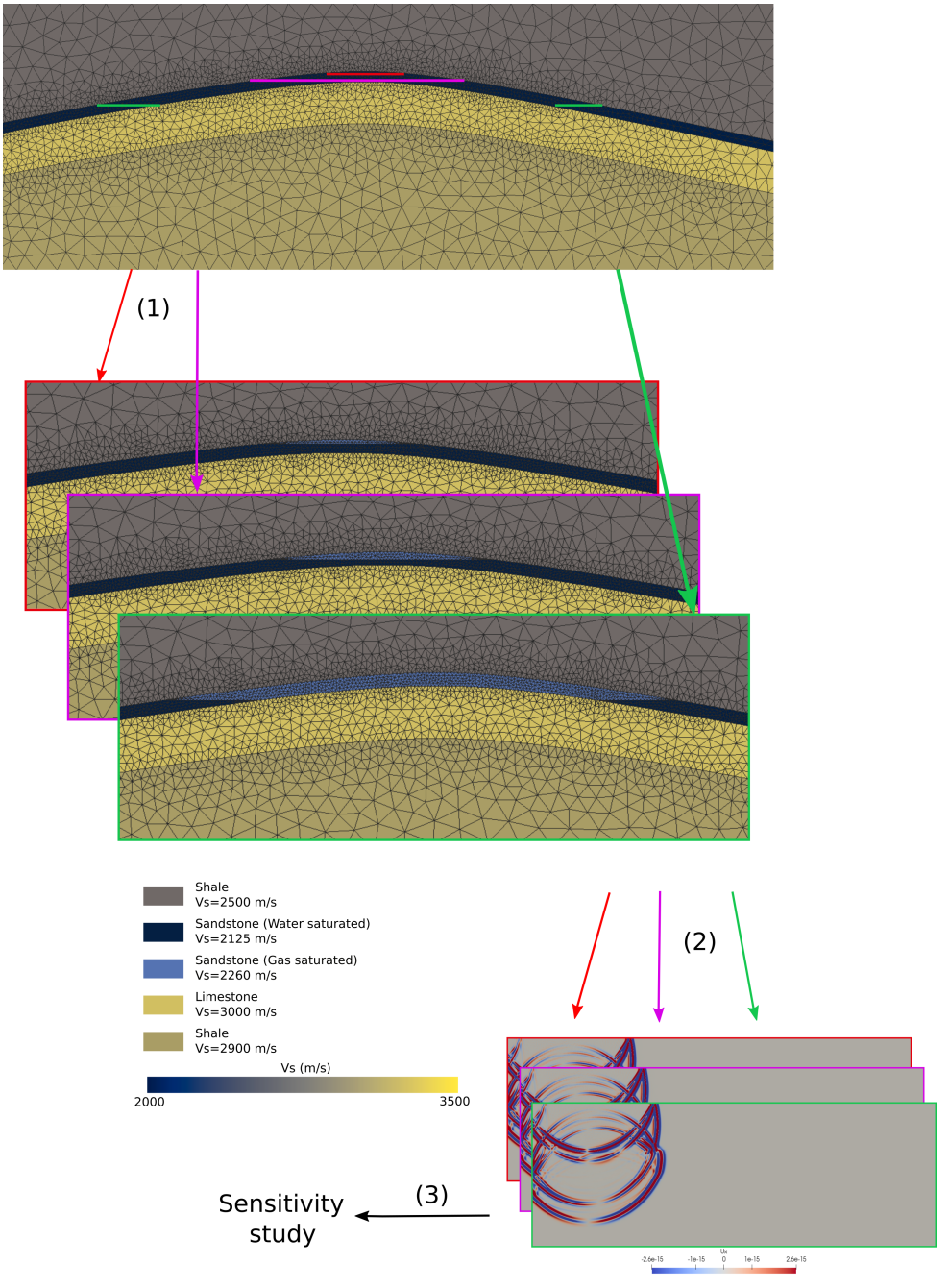

Figure 1: (1) From several level-sets defining the possible interface positions between water-saturated sandstone and gas-saturated sandstone, we use Mmg (Dapogny et al., 2014) to locally remesh a selected layer (dark blue) and (2) the Hou10ni2D software (Barucq, 2016) to simulate wave propagation and (3) compare the simulation results.

2. State of the art

Definitions Physical modeling in the subsurface generally involves the construction of a geological model representing the interfaces between rocks that have different physical properties (such as porosity, permeability, density, Young

modulus, shear modulus) (Ringrose and Bentley, 2015; Wellmann and Caumon, 2018). These properties depend on multiple factors (e.g., facies, fluid saturation, compaction, temperature). Geological models, therefore, are multi-material models, a term used more generally in mechanics. The interfaces between different materials correspond to horizons, faults, unconformities, intrusions, cavities and fluid contacts. Among the various possibilities to represent geological media, unstructured meshes offer the interesting ability to honor complex geometries and to spatially vary the level of detail. In previous works, 3D models have been considered, but for simplicity here we consider triangulated two-dimensional geological models similar to those defined in Anquez et al. (2019) or Pellerin et al. (2017) (Figure 2). Indeed 2D models are most effective for proof of concept, as they allow to assess the impact of changes on physical simulation in acceptable time (Section 4.1) and they are commonly used for physical models in cylindrical domains. Generalization to 3D will be discussed in Section 5.

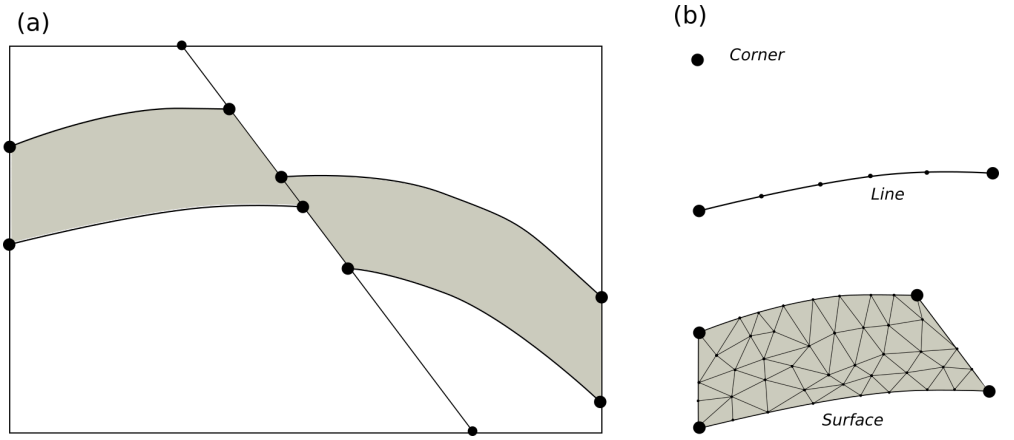

Figure 2: 2D triangulated models are defined by their Corners (black dots), Lines, and Surfaces (a) whose geometry is supported by points, segments and triangles (b)

Triangulated models are adequate to run wave simulations with a Discontinuous Galerkin method provided that the mesh is valid and of sufficient quality. By valid we mean that all intersections between two triangles of the mesh are either empty or a common edge/vertex to both triangles and that no element is empty. The quality of the mesh is related to the size and shape of the triangles. It has an impact on the accuracy and computation time, and its definition is specific to each solver (e.g., Loseille et al., 2010). The interfaces between two materials are represented by discretized lines that separate two regions of the model. An alternative representation of interfaces in geological modeling, and more generally in multi-material modeling, is the level-set representation (also called implicit). In geological modeling this representation has gained popularity and is the base of the implicit stratigraphic modeling. In this context, the scalar field representing stratigraphy in a conformal layer can be seen as relative geological time (Caumon et al., 2013; Collon and Caumon, 2017; Chilès et al., 2004; Houlding, 1994; Ledez, 2003; Mallet, 2004; Tertois and Mallet, 2007). In some cases, level-set interfaces can be directly integrated in physical solvers using Heaviside basis functions as in XFEM

(Moës et al., 2002) or to define specific boundary conditions (e.g., Durand-Riard et al., 2010). Level-set representation has also gained popularity to solve subsurface inverse problems (e.g., Cherpeau et al., 2012; Giraud et al., 2021; Guillén et al., 2008; Zheglova et al., 2018).

Editing models Different types of local modifications are described in the literature. Some authors propose to locally deform the mesh using geometric methods (Laurent et al., 2015; Tertois and Mallet, 2007). These constrained deformation methods are based on the definition of a smooth deformation field interpolated from a few anchor points. One of the problems encountered when modifying the geometry of a set of vertices in a mesh is that the elements may become invalid, as some intersections may occur between the edges of the triangles or the faces of the tetrahedra (Tertois and Mallet, 2007).

However, general displacement, insertion and removal of boundaries lead to more substantial topological changes affecting all model entities (nodes, edges, regions). Sword Jr (1991) proposes methods to edit and update the object adjacencies and to verify the model topological validity at each modification (edge intersection verification, for example). In 3D, Euler et al. (1999) propose a general way to edit boundary representations which relies on intersections and border projections of triangulated surfaces before globally reconstructing a boundary representation. Although this approach is very flexible in principle, the use of projection raises instabilities and the approach does not provide a strict guarantee that the model integrity is maintained throughout the editing. As part of the update of geomodels during drilling monitoring, Suter et al. (2017) propose to modify the only geological block involved in the new data which does not correspond to the initial model. The region to modify is completely erased and meshed again taking into account the new data (Figure 3), but mesh conformity, required in most physical simulation codes, is not discussed.

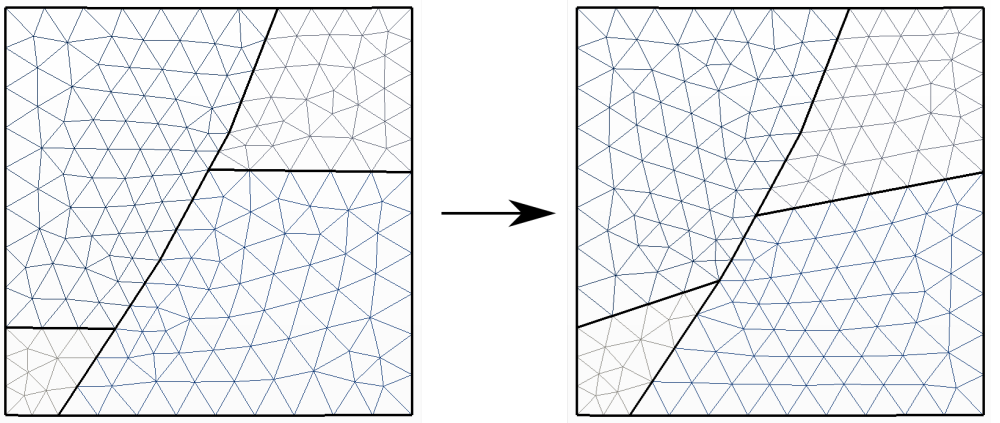

Figure 3: Example of a fault throw modification in which the model is completely erased and meshed again.

We follow a similar strategy in this work, but we also capitalize on recent advances in shape optimization that regroups a set of methods for finding the “best shape" of an object so that it fulfills its functions. This optimization is

automated and the geometrical modeling also uses unstructured meshes. The management of heterogeneity as present in geological models, introduces specific difficulties compared to the optimization of homogeneous objects (Wang et al., 2015). Level-set methods are very interesting because they allow tracking fronts and free boundaries. Sethian and Wiegmann (2000) first introduced the level-set description into topology optimization. Level-set techniques were then developed in, e.g., Allaire et al. (2004), Osher and Santosa (2001), Sethian and Wiegmann (2000),Wang et al. (2003) to perform topological changes of the level-set components. An interface Ω is defined by an iso-value φ_0 of a level-set function (i.e, a scalar field) φ as

$$\Omega = \left\{\overline{x}, \varphi(\overline{x}) = \varphi_0\right\}. \tag{1}$$

This level-set representation is able to represent geometric interfaces between materials, such as geological interfaces, as shown in Figure 4. Allaire et al. (2014) propose to explicitly discretize the level-set at each iteration in a computational domain equipped with a simplicial mesh. In doing so, a sub-mesh of the domain is created at each step.

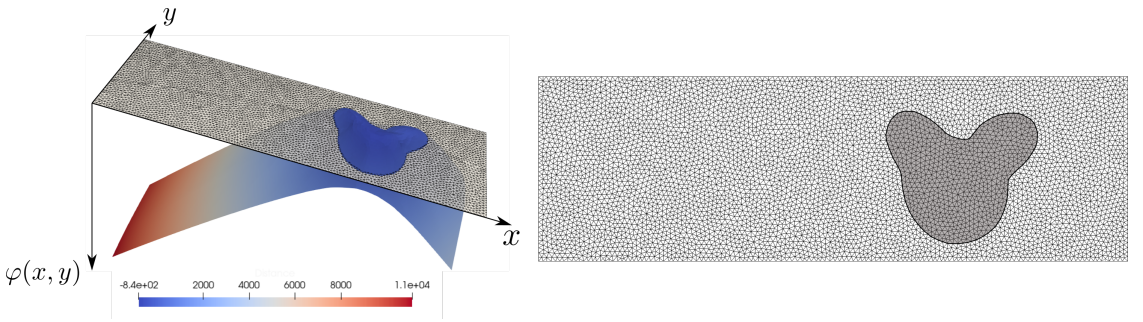

Figure 4: (Left) 2D level-set function; (right) a corresponding meshed description: the 2D domain is equipped with a mesh (composed of the white and grey elements). The iso-value 0 represents the interface between the white and grey regions.

In the shape optimization by a physical constraint, the accuracy of the border has a direct impact on the precision of the simulations. To build the obstacle boundaries, Santosa (1996) proposes an inverse approach involving a set of level-set functions that minimizes a residual to fit data. To deal with multi-material models, Wang et al. (2005) and Wang et al. (2015) introduce a “color” level-set method, where each material is defined by a level-set function. This approach is similar to a subsurface inverse problem considering, for example, the position of a horizon as a parameter set. To solve an inverse problem in full waveform case, Guo and de Hoop (2013) adapt the method of Santosa (1996) and use concepts from shape optimization and image segmentation to determine the position of a salt body. Giraud et al. (2021), and Zheglova et al. (2018) use multiple level-sets to represent multiple geological units in a model, therefore can recover the geometry of geological bodies using level-set inversion of geophysical data.

3. Implicit local interface insertion

In this section we propose to insert a level-set interface in a mesh by restricting the modifications to a prescribed region of the model. The chosen level-set iso-value is first discretized, and the modified region is remeshed conformably to prevent a steep decrease of the mesh quality that would slow down further computations or make them unstable. When merging the edited region with the other parts of the model, specific care to preserve the mesh conformity is taken.

3.1. Input Data

Level-set function To perform the local insertion of an interface in the geomodels, the input data is composed of the global mesh and the interface implicitly defined (e.g, a fault, a gas-water contact...). In our case, the level-set is approximated by the iso-values of a regular piecewise linear scalar field represented on the nodes of the triangular mesh. Typically, the scalar field represents the signed distance to the line, which is defined by the 0-valued segment in each intersected triangle (Figure 5b, Figure 6b). The insertion of the new points and edges is based on this implicit line definition.

Model partitioning In our method, the area to be modified (inner region) consists of one or several input surfaces representing geological units, but this can easily be changed to a list of triangles, e.g., to insert an internal fracture. The implicit line will be inserted in the inner region while maintaining the conformity to the lines and corners of that region, e.g., the blue layers (# A1, A4, B2 and B3) in Figure 6a. The rest of the model (outer region), is not affected by the modification, except a small set of triangles which needs to be modified to maintain the model conformity. In Figure 6a, all the triangles of the outer region that are in contact with the bold boundaries could be affected by this conformity requirement; in practice, as will be further explained in Section 3.2.3, only the triangles that are in contact with the level-set need to be considered.

3.2. Local level-set discretization

3.2.1. Mmg software

We use the Mmg code for the level-set insertion in the inner region. Mmg is an open source 2D and 3D remeshing software with two major features: level-set discretization and mesh adaptation. Mmg is dedicated to the processing of triangle and tetrahedral meshes. It is a meshing software mainly used for computational fluid dynamics applications and for shape optimization applications (Benard et al., 2016; Loseille et al., 2010). It has also recently been effectively integrated to adapt meshes in full waveform inversion problem to accelerate the computations (Jacquet, 2021).

The discretization of level-sets allows to insert a line or a surface that represents a scalar field iso-value in a mesh. The scalar field is defined at all the nodes of the mesh, forming a piecewise linear function. The software takes

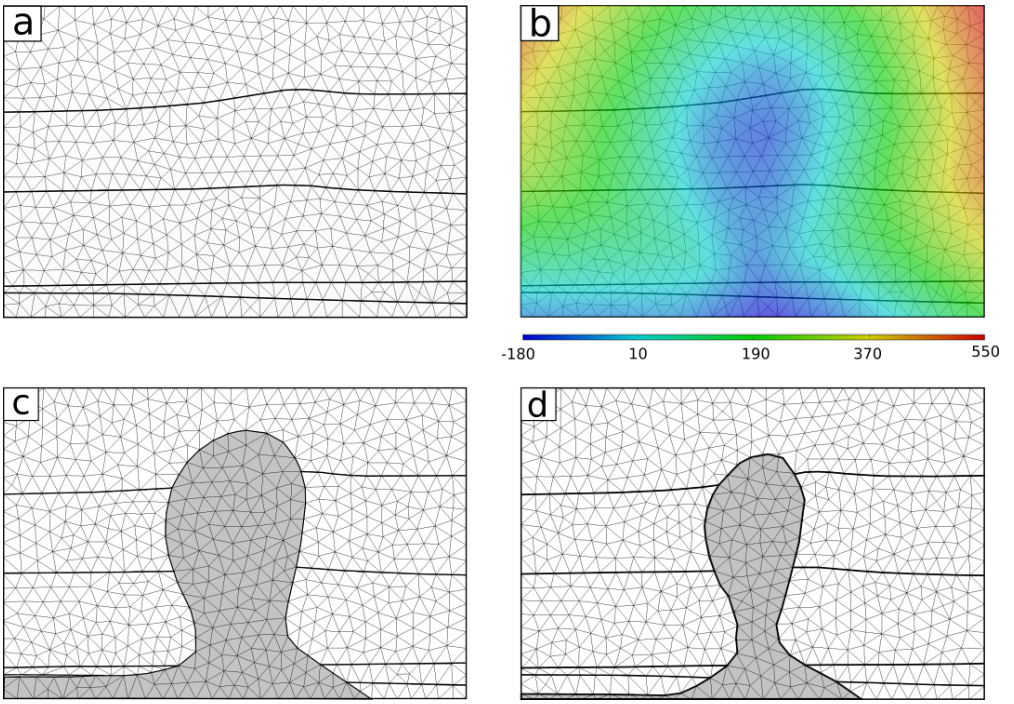

Figure 5: Insertion of an implicitly defined salt dome (b) in a geological model (a). The iso-values of the signed distance scalar field represent possible salt dome boundaries; (c) and (d) show two resulting models for scalar values 0 and -70, respectively.

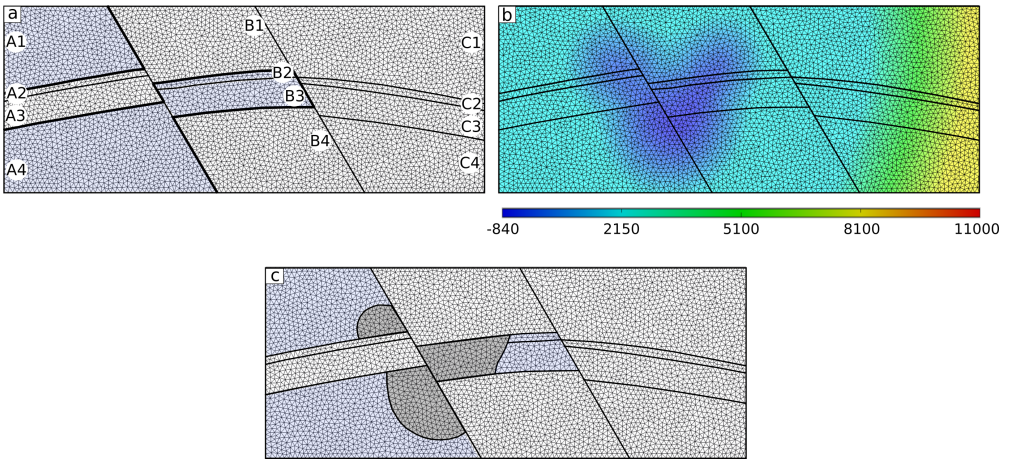

Figure 6: The flexibility of the proposed approach demonstrated on the insertion of an arbitrary shape in an edited region composed of surface units A_1, B_2, B_3 and A_4 (light blue).

into account multi-material models, so the discretization of the iso-value can be limited to determined materials and maintain existing materials.

The other main feature of Mmg is the mesh adaptation: the user can set several parameters to control the size of the mesh elements. For example the *hmin* and *hmax* parameters are used to define the minimum and maximum size of the elements; the parameter *hgrad* controls the ratio between the length of two adjacent edges. The user can set

several command line parameters or provide an input size map to control the size of mesh elements.

3.2.2. Level-set discretization

The mesh modifications are made with the level-set discretization method. The algorithm implemented in Mmg (Dapogny et al., 2014) consists of two main steps. First, the line is inserted in the defined region as simply as possible while keeping the mesh consistent: each triangle intersected by the level-set is cut into either two triangles (when the level-set goes exactly through one vertex) or one triangle on one side and two triangles on the other side (when the level-set cuts the interior of two edges) (Figure 7). However, most of the newly created triangles are of poor quality (Figure 8.a.), so remeshing is essential before running a seismic simulation.

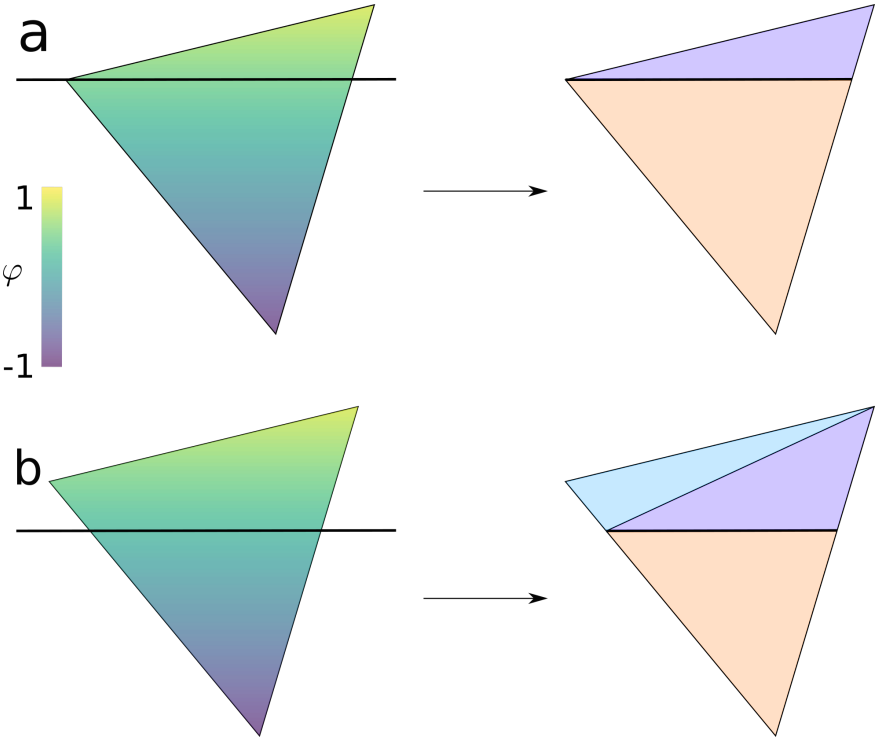

Figure 7: Two steps level-set discretization method in Mmg: (a) If the level-set goes exactly through one vertex, the triangle is cut into two triangles; (b) if the level-set cuts the interior of two edges, the triangle is cut into one triangle (red) on one side and two triangles (green and blue) on the other side

In the interface discretization, the major constraint is to guarantee the conformity of the entire mesh for both the inserted and pre-existing boundaries. To this end, only the triangles adjacent to the modified region and in contact with the ends of the implicit interface are modified. They are simply divided into two new triangles (Figure 9).

The inner region is then divided into two regions corresponding to the two sides of the inserted interface. The two parts of the mesh are remeshed separately to adapt the mesh to the constraints imposed by the user: the maximum or minimum element size and the gradation (i.e., the ratio of adjacent elements size). The operations performed on

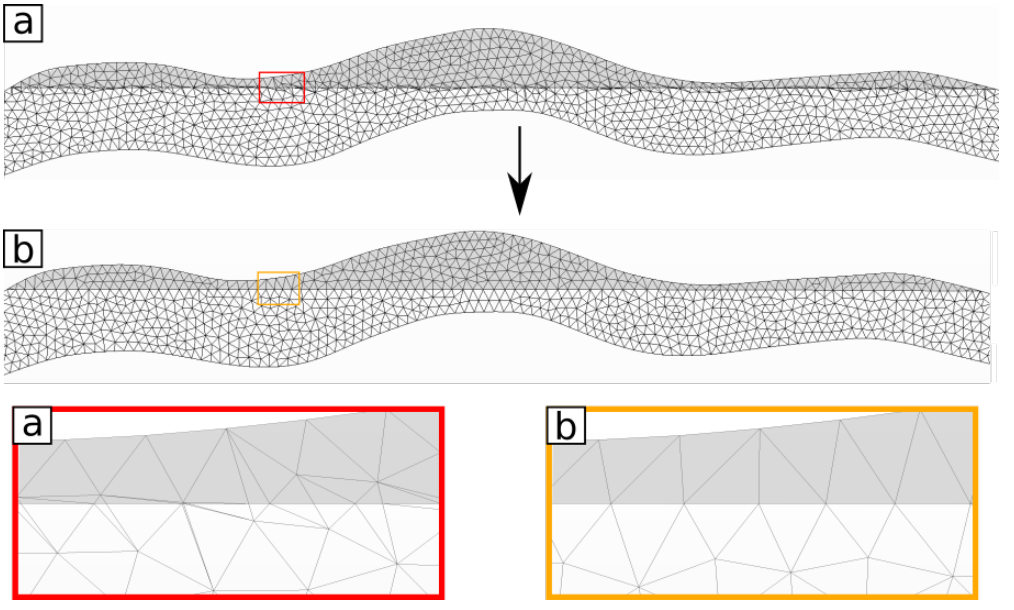

Figure 8: Two steps level-set discretization method in Mmg: (a) insertion of the line by creating new nodes and triangles; (b) remeshing of the region

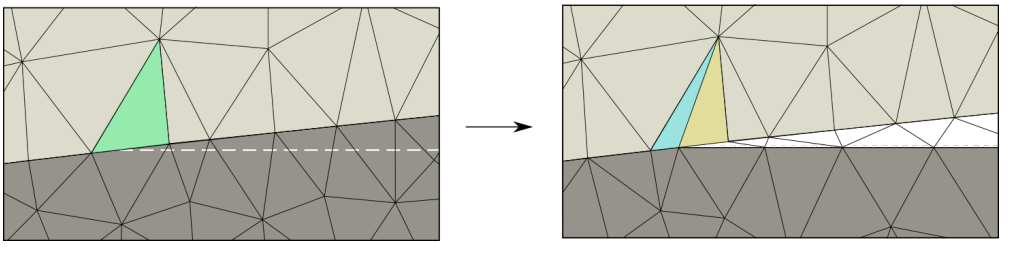

Figure 9: Division of a triangle at the edge of the modified region to maintain the mesh conformity

the mesh consist of insertion or displacement of nodes, edge swap or collapse. All decisions are made to adapt to the size map defined as input and to improve the mesh quality. To maintain the conformity of the overall mesh, the edges between sub-parts must not be modified (Figure 8b).

3.2.3. Merge

The last step consists in merging the modified and remeshed region and the preserved one. During this step some points are duplicated. The mesh cannot have points at the same position for our wave propagation simulation. Duplicated nodes are removed by using co-location detection from Gmsh[1]. This API function is based on a R-Tree (Guttman, 1984).

[1] https://gitlab.onelab.info/gmsh/gmsh

3.3. Mesh quality

To evaluate the mesh quality we propose to compute the minimal height of the worst element among the n_t triangles:

$$Q = \min_{\forall k \in [\![1;n_t]\!]} h_k, \tag{2}$$

where h_k is the lowest height of the triangle k. The quality Q has an important impact on elastic wave simulation time because of small time steps imposed by the Courant–Friedrichs–Lewy (CFL) condition (Section 4.2). To minimize the decrease of quality, if the distance between the level-set and a node located on another interface is less than a given tolerance ϵ, the scalar field is locally modified: the iso-value is set at this existing node so that no new node is created during the line insertion in Mmg (Figure 10). In Figure 10, the difference of the scalar field values of two vertices in a triangle $|\varphi_1 - \varphi_0|$ is normalized by the norm of gradient of the level-set function in the triangle $||\vec{\nabla}\varphi||$. This value is then compared to the tolerance ϵ that can be assimilated to a distance. By adjusting the parameter ϵ, one can limit the creation of very elongated triangles which otherwise appear at the intersection between the iso-value and the borders of the layer, at the expense of a small inaccuracy in the final geometry.

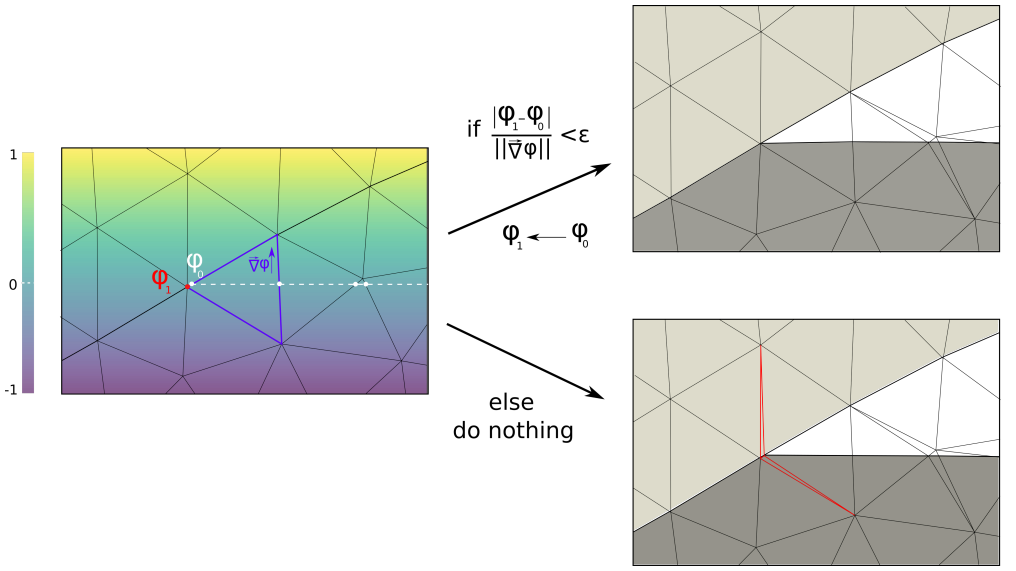

Figure 10: During the level-set discretization, if the distance between the iso-surface and an existing node is less than ϵ (2), the iso-value is approximated at this point and no other point is created when this approximation is not made, ill-shaped triangles are formed (in red).

3.4. Open-Source Implementation

Process automation We propose algorithms for the automation of the process. The code is available on Github[2] and depends on Mmg[3] (Dapogny et al., 2014) and Gmsh[4] (Geuzaine and Remacle, 2009). It allows to create the two sub-meshes to restrict the discretization to the modified region, and then to merge them. Duplicated nodes are removed by co-location detection from Gmsh. It is then possible to create models that correspond to the input format of the simulator. To prevent remeshing of the entire mesh, the options *-nomove*, *-noinsert*, *-noswap* are used on the command line when calling Mmg for level-set discretization. The *-nomove* option blocks the movement of vertices and the *-noinsert* one prevents the creation of new vertices. The *-noswap* option prevents the edge swapping between two adjacent triangles.

Element quality improvement A large part of finite element schemes solving boundary values problems imposes the absence of triangles whose edges are on two different borders of the model (Figure 11). In our application, the edges are not domain boundaries but only material boundaries, hence they do not carry boundary conditions. Therefore, we activate the *-nofem* option in Mmg to improve the mesh quality. The options *hmin* and *hmax* can also be used to set the mesh size to adapt the mesh to the physical simulator.

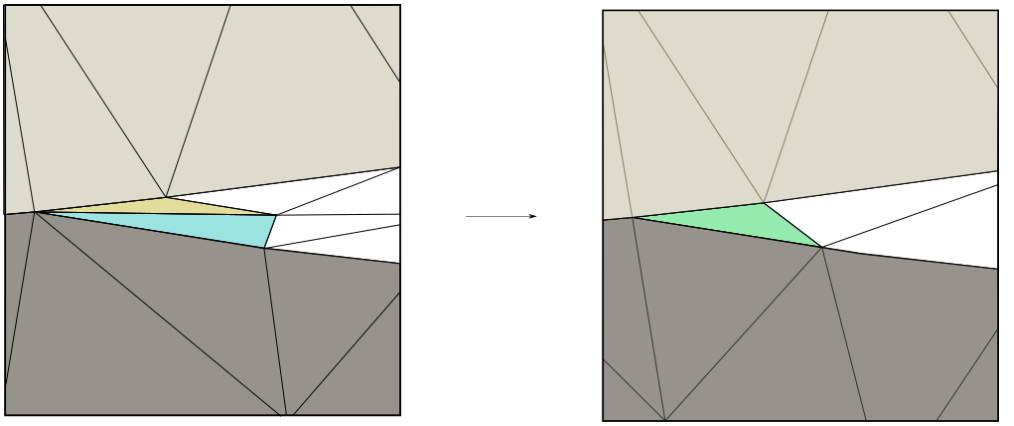

Figure 11: Results of MMG remeshing by default (left) and with the option *-nofem* activated (right). With this option, triangles with two constrained edges are allowed, yielding a higher quality mesh for our application.

However, there are very thin objects in geology, which inevitably yield poor quality triangles. During the physical simulations, such triangles show a very small value of the determinant of their Jacobian matrix, leading to potential inaccuracy in the simulation result. In dynamic problems, these triangles also imply a small time-step because of the CFL condition, which impacts the computational cost. Additionally, it could be combined with approaches to simplify models in order to reduce the simulation time. For example, during the level-set discretization, an option *-rmc* is

[2]https://github.com/ring-team/LUMOS2D
[3]https://github.com/MmgTools/mmg
[4]https://gitlab.onelab.info/gmsh/gmsh

available to remove small surface parts. The decision is taken by comparing the surface of the small component to the region surface.

For each new model created, the mesh quality (2) is computed. If the quality is too low (the choice of the quality threshold is discussed in Section 5), the process can be repeated after approximating the scalar field at several nodes by increasing ϵ to avoid problematic configurations (Figure 10, Figure 14). A new model is then created with less elongated triangles.

File format Mmg uses the Medit file format (*.mesh*). We use the tag that may be set on the elements to encode model entities. The scalar field and/or metric for remeshing values are defined on the vertices of the mesh and are stored in an other file format (*.sol*). The local parameters for multi-material models are defined in a 2 dimensional Mmg file (*.mmg2d*).

4. Gas-water contact uncertainty and elastic wave propagation

In this section, we apply our local level-set based model edition to evaluate the impact of a gas-water contact depth on seismic signals. We consider a synthetic model on which we quantitatively seek to evaluate the correlation between the contact depth and some seismic waveform misfits, demonstrating the usefulness of our approach to efficiently sample and reduce uncertainties on a material interface position.

Our synthetic geological model M_{ref} is an anticline overlying horsts and grabens (Figure 12). The anticline is composed of folded layers of shale and sandstone. After the insertion of the gas-water contact in the reservoir, the gas zone is represented in grey (layer 6 in Figure 12). The domain size is 16.2 km horizontally and 5 km vertically. The petrophysical values of the different layers of the model are summarized in Table 1. These values were chosen consistently with the case study of Hamada (2004). For simplicity, we use a constant density $d = 2600\, kg/m^3$.

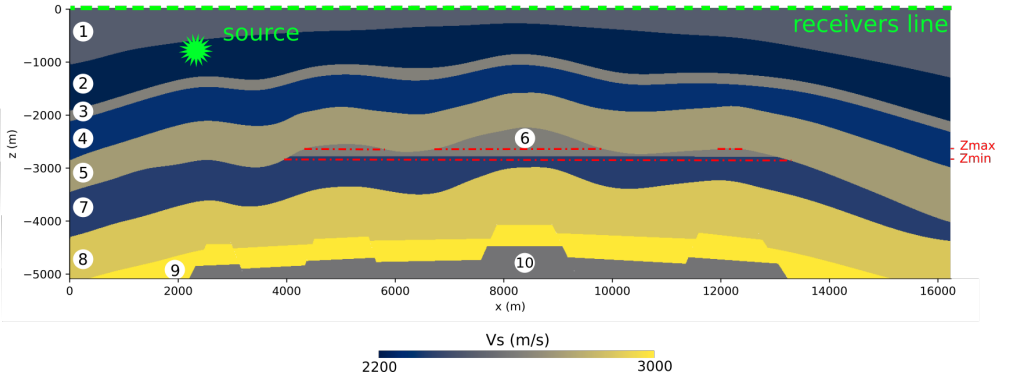

Figure 12: Reference model: the gas-water depth is $z = -2,785\, m$. The dashed green line represents a line of 150 receivers (one every 100 m) at the top of the domain. The lithology is presented in Table 1

Color map	Lithology	P-wave velocity (m/s)	S-wave velocity (m/s)
1	Shale	3000	2500
2	Sandstone	3400	2260
3	Shale	3200	2650
4	Sandstone	3500	2330
5	Shale	3300	2750
6	Sandstone (Gas sat.)	3700	2740
7	Sandstone (Water sat.)	3800	2375
8	Shale	3900	2600
9	Limestone	4000	2900
10	Sandstone	4500	3000

Table 1
Lithological and petrophysical characterization of the model Figure 12. Density is constant $d = 2600\,kg/m^3$.

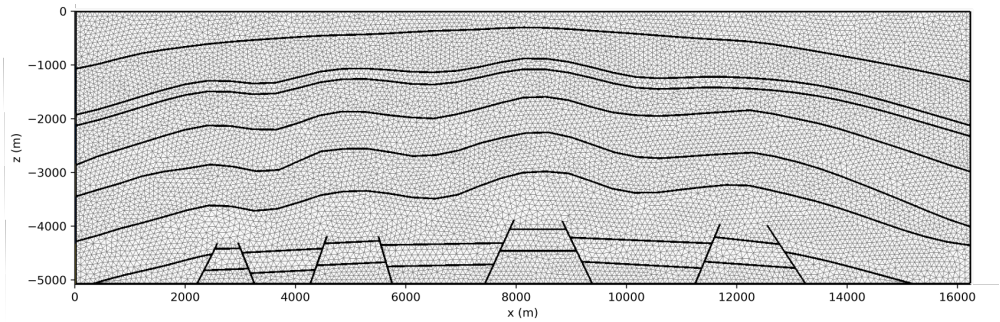

Figure 13: The initial mesh of our synthetic model generated with Gmsh and Mmg, contains 22,077 triangles.

4.1. Seismic simulation parameterization

In this study, we use the Hou10ni2D software (Barucq, 2016) which implements a Discontinuous Galerkin (DG) method (Reed and Hill, 1973) for solving the wave equation. More precisely, Hou10ni2D relies on Interior Penalty approach (Grote et al., 2006; Riviere, 2008) to simulate time-dependent elastic wave propagation. Hou10ni simulates seismic wave propagation in heterogeneous media and allows the use of different polynomial orders in the mesh elements (p-adaptivity in space) (Barucq et al., 2014). In addition, Hou10ni2D can run on parallel architectures.

We apply absorbing boundary conditions on the two lateral sides and the bottom of the cross-section, whereas the top of the domain is defined as a free surface. We choose the source time-function as a Ricker wavelet with a dominant frequency $f = 15\,Hz$. As a consequence, the minimum wavelength is

$$\lambda_{min} \simeq \frac{v_s}{3f}, \tag{3}$$

Depth (m)	Nb triangles	Quality	Time (s)	Nb CC
-2,645	21,997	8.54	17,321	3
-2,655	21,989	2.00	46,376	3
-2,665	22,007	6.37	16,973	3
-2,675	21,997	6.1	18,231	3
-2,685	21,995	2.35	42,651	3
-2,695	22,023	4.85	21,300	3
-2,705	22,003	4.76	21,759	2
-2,715	21,971	5.1	20,847	2
-2,725	22,003	7.99	18,469	2
-2,735	22,011	2.95	33,718	2
-2,745	21,991	6.01	19,620	1
-2,755	21,967	25.51	11,348	1
-2,765	21,997	2.77	35,271	1
-2,775	21,981	22.76	10,809	1
-2,785	21,959	7.36	20,298	1
-2,795	21,969	17.95	11,508	1
-2,805	21,971	24.84	11,514	1
-2,815	21,939	11.31	13,674	1
-2,825	21,955	6.89	17,883	1
-2,835	21,951	2.57	38,380	1
-2,845	21,959	22.55	11,015	1

Table 2
Model characteristics (Contact depth, number of triangles, worst element quality, simulation time and number of connected reservoir parts). The quality is the minimal triangle height (2). Simulations are run on a machine with a processor Intel(R) Xeon(R) CPU E5-1620 v2 @ 3.70GHz, 8 Cores.

where v_s is the S-wave velocity. The source is located at depth $z = -775\,m$, two kilometers from the left side. We place a line of 150 receivers (one every 100 m) at the top of the domain (dashed green line in Figure 12). Simulations are run for $T = 4\,s$ after the shock. The displacement is computed for all the receivers at each time step.

4.2. Comparison of simulation results with a varying gas-water contact depth

Set of models We built 20 models by inserting the gas-water contact at several depths in the initial mesh Figure 13, using our method presented in Section 3. The process takes about 10 seconds per model. Depths vary from $z_{min} = -2,845\,m$ to $z_{max} = -2,645\,m$ (between the two dashed red lines in Figure 12), with a constant step δz equal to 10 m. Each model is characterized (Table 2) by the contact depth, number of triangles, mesh quality, simulation time, and number of connected reservoir parts (Nb CC in Table 2). To evaluate the quality, we chose the minimal of all triangle heights (2), as it is directly linked to the software heuristics for the determination of the time step and the level of the p-refinement. This value has a strong impact on the simulation run time of simulation as can be seen in Figure 14.

Impact of quality on simulation time The mesh quality depends on the model geometrical configuration. There is no direct link between the worst element quality, the depth of the contact or the number of connected components of the gas-saturated layer (#6 in Figure 12). Poor quality triangles are located around the ends of the gas-water contact line. They often are small and elongated triangles. The existence of these ill-shaped triangles is partly a consequence of

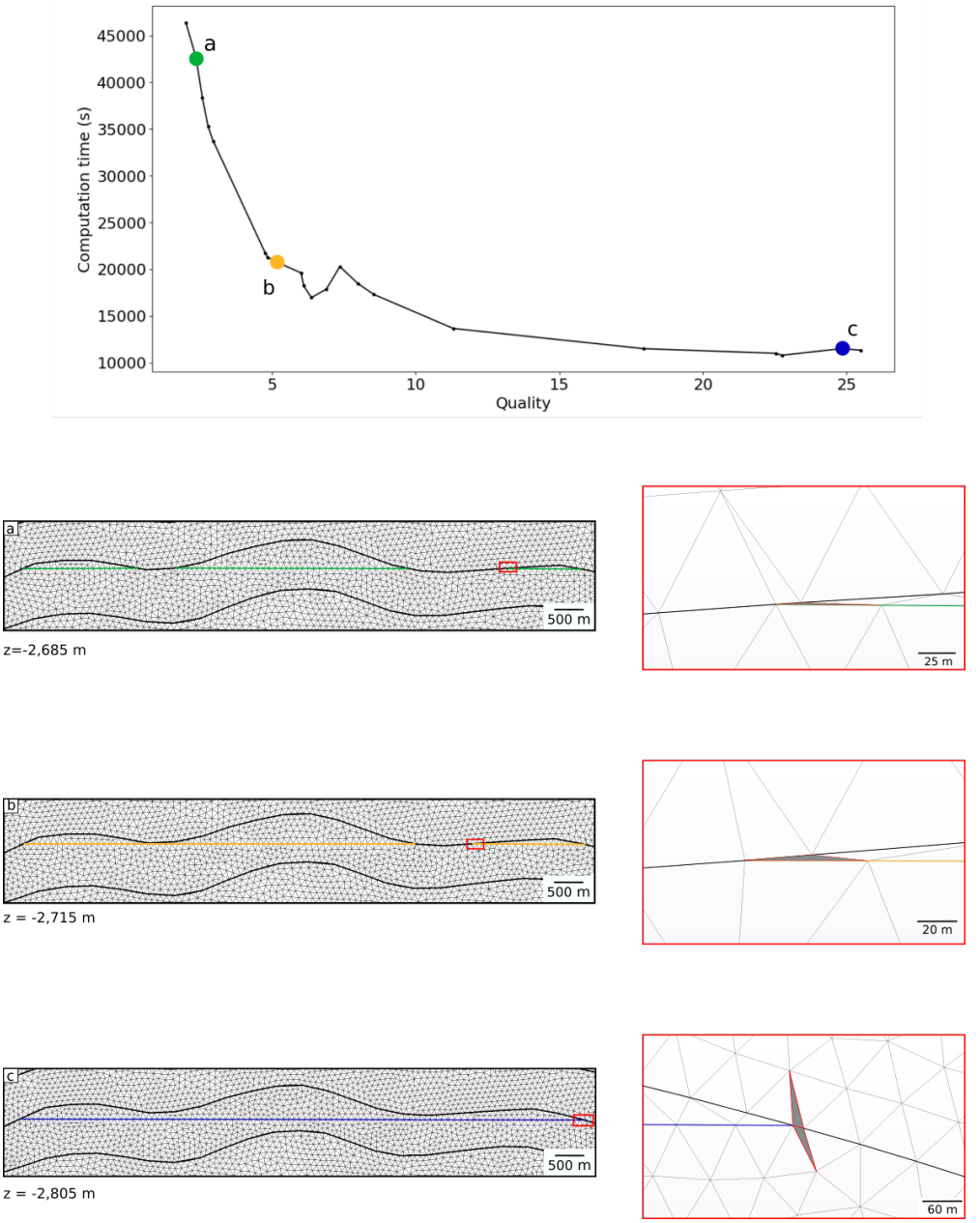

Figure 14: The mesh quality impacts the computation time: the highlighted triangles with the lowest quality (right) for 4 models (left) have elongated form, leading to decreasing time steps and increasing simulation run time (top).

low angles between the contact and stratigraphic boundaries (close-up views in Figure 14b and Figure 14c). However, the position of the new corners is the parameter that most impacts the mesh quality and the simulation time. If the corner is very close to a vertex of an adjacent triangle of the outer region (#5 in Figure 12), the quality of the triangles created is low (Figure 14a and b). The approximation of the scalar field described in Section 3.2 and Figure 10 avoids the creation of very poor quality triangles.

Depth (m)	Scalar field approximation	Quality	Time (s)
-2,705	$\epsilon = 0$	0.04	>2,000,000
	$\epsilon = 0.5\,m$	4.76	21,759
-2,775	$\epsilon = 0$	0.74	129,102
	$\epsilon = 0.5\,m$	22.76	10,809

Table 3
Impact of elongated triangles deletion: the simulation time is between 12 and 95 times shorter. Simulations are run on a machine with a processor Intel(R) Xeon(R) CPU E5-1620 v2 @ 3.70GHz, 8 Cores.

The scalar field has been locally approximated for two models: $z = -2,775\,m$ and $z = -2,705\,m$ with $\epsilon = 0.5\,m$. These small modifications lead to a large quality improvement and a significant reduction of the computation time (Table 3).

Comparison with the reference model For each modified model $\mathbf{M_z}$, a simulation is run using the corresponding velocity model. Then the relative difference $\delta d_{i,z}$ at each receiver i between the seismogram $\overline{u}_{i,ref}$ of the reference model $\mathbf{M_{ref}}$ (Figure 12) and the seismogram $\overline{u}_{i,z}$ simulated in each model $\mathbf{M_z}$ is calculated (Geller and Takeuchi, 1995):

$$\delta d_{i,z} = \left(\frac{\int_0^T \left\| \overline{u}_{ref}(t) - \overline{u}_{i,z}(t) \right\|^2 \mathrm{d}t}{\int_0^T \left\| \overline{u}_{ref}(t) \right\|^2 \mathrm{d}t} \right)^{\frac{1}{2}} \tag{4}$$

The results are difficult to interpret because the simulated wavefield is complex. From Figure 15, we see that the largest waveform difference ($\delta d_{i,z} > 20\,\%$) is obtained between $x = 5,200\,m$ and $x = 13,400\,m$. On average, the seismogram error increases when the contact depth error Δz increases. Horizontally, however, Figure 15 shows that some receivers are not sensitive to contact depth uncertainty, e.g., from $x = 0\,m$ to $x = 2000\,m$ and from $x = 13,600\,m$ to $x = 15,000\,m$. This corresponds to receivers for which the possible contacts are not illuminated by the wavefield. Interestingly, we also observe that the local error decreases with increasing depth differences, e.g. from $x = 6,500\,m$ and $x = 7,500\,m$ with $\Delta_z > 110\,m$. This highlights the importance of the starting model to solve inverse problems from sparse seismic measurements to avoid being trapped in local minimum when only a few receivers are used. Due to the complexity of these results, a comparative analysis on a single receiver is delicate, and it is more relevant to take into account the seismograms at a large set of receivers to analyze the results.

To more easily compare simulations we choose a unique indicator, namely the mean μ_z of the errors on the n

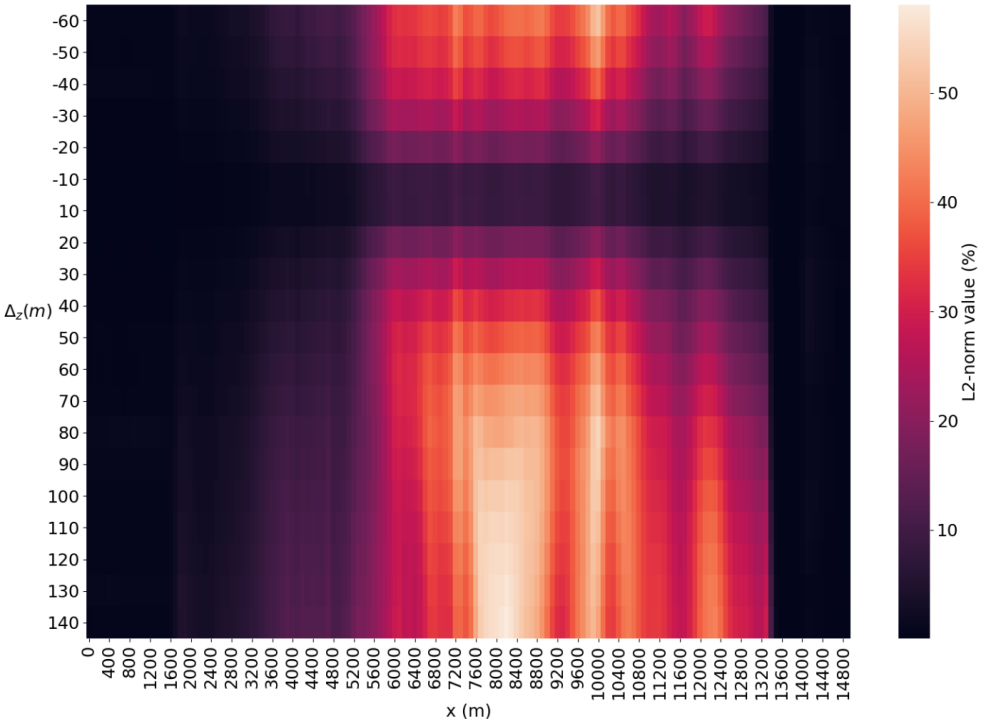

Figure 15: L2-norm waveform difference $\delta d_{i,z}$ (4) for each receiver i at position $x = i * 100\,m$ as a function of contact depth difference Δ_z (results are in percentages). The color represents the L2-norm value at one receiver for one Δ_z. The Δ_z values are negative when the contact of a model is below the contact of the reference model.

receivers:

$$\mu_z = \frac{\sum_{i=0}^{n} \delta d_{i,z}}{n} \tag{5}$$

We observe in Figure 16 a correlation between the mean error and the depth error Δz : the larger the distance from the reference depth contact, the higher the mean of L2-norm.

The inverse problem we consider consists in finding a model $\mathbf{M_z}$ containing a contact at the depth z, such that its seismic response $s(z)$ is "close" to a reference seismic response, obtained from the model $\mathbf{M_{ref}}$ defined as $s(z) = s(z_{ref})$. The difference in seismic response is evaluated using the L2-norm (4 and 5). The inversion loop to determine the best model that fits the seismic response of the reference model is, in general, a difficult process. To solve a Bayesian inverse problem, many different models have to be generated and seismic simulations are required for each of them. Here, the inversion only concerns one parameter (the contact depth), so we use a simple grid search (brute-force) approach using the previous results (Figure 15 and Figure 16).

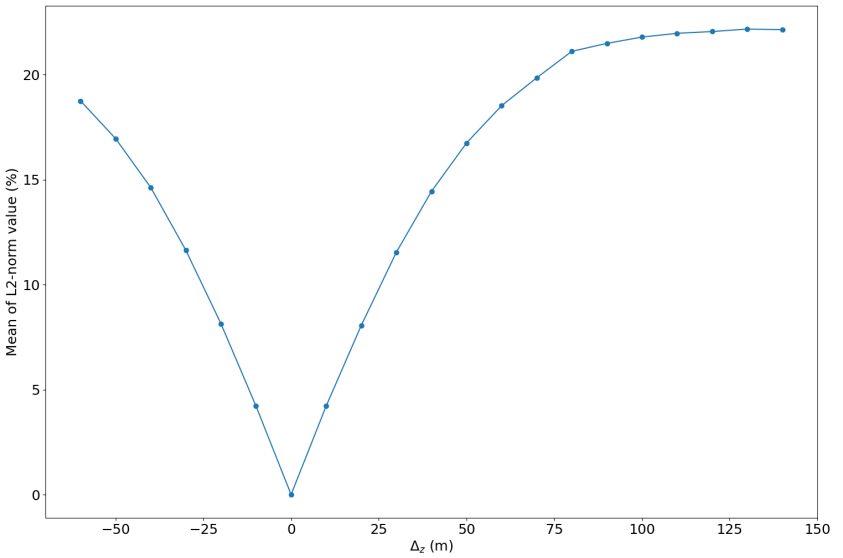

Figure 16: Mean of L2-norm μ_z (5) as a function of Δ_z

4.3. Quantification of uncertainties

To test the impact of the modifications on the simulations, and to study the feasibility of integrating our approach in an inversion loop, we compute the density of probability describing the depth of the contact. Bayes theorem (e.g., MacKay, 2003) is used to combine prior information on the structural model with the observed data to give the posterior probability density function

$$\rho(z|\mathbf{D}) = \frac{\rho(z)L(\mathbf{D}, z)}{\int_z \rho(z)L(\mathbf{D}, z)\mathrm{d}z} \tag{6}$$

where $\rho(z)$ is the prior probability density, i.e., the information we have on the contact depth before considering the data $\mathbf{D}$. In this study, we choose a non-informative (uniform) prior probability density

$$\rho(z) = \begin{cases} \frac{1}{z_{max}-z_{min}} & \text{if } z \in [z_{min}; z_{max}] \\ 0 & \text{otherwise} \end{cases}. \tag{7}$$

The likelihood function $L(\mathbf{D}, z)$ quantifies how equivalent a candidate model $\mathbf{M}$ is to the reference model $\mathbf{M_{ref}}$ by comparing their seismic simulation results: $\mathbf{D}(z)$ at all receivers for the candidate model and $\mathbf{D}_{ref} = \mathbf{D}(z_{ref})$ for the

reference model. In this work, we use a classical Gaussian assumption:

$$L(\mathbf{D}, z) = \rho(\mathbf{D}|z) = \frac{e^{-\frac{1}{2}\frac{\left\|\mathbf{D}(z)-\mathbf{D}_{ref}\right\|^2}{\sigma^2}}}{\sigma\sqrt{2\pi}}, \text{ with } \sigma = \|\mathbf{D}\| \tag{8}$$

This makes it possible to use the values of L2-norm introduced in the previous section to calculate the posterior density of probability. By using (4) to simplify (8) we obtain

$$\frac{\left\|\mathbf{D}(z) - \mathbf{D}_{ref}\right\|^2}{\sigma^2} = \sum_i (\delta d_{i,z})^2 = \Delta d_z^2, \tag{9}$$

$$\tag{10}$$

and then

$$L(\mathbf{D}, z) = \rho(\mathbf{D}|z) = \frac{e^{-\frac{1}{2}\Delta d_z^2}}{\sigma\sqrt{2\pi}} \tag{11}$$

The posterior probability density function is computed for the set of models and we obtain the results presented in Figure 17. We can see that the density of probability is maximum around the reference depth. More generally, such a density of probability quantifies the posterior uncertainties on the depth of the contact.

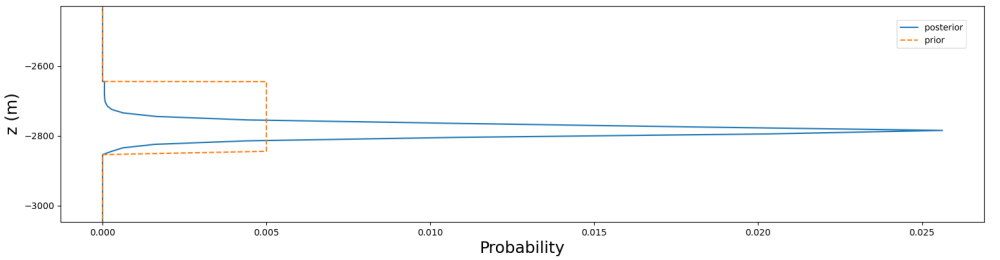

Figure 17: Posterior probability density function. The density is maximal around the reference depth $z = -2,785\,m$. The most probable gas-water contact depth can therefore be determined in the proposed settings.

5. Discussion and conclusion

In this paper, we have proposed a method to locally modify a meshed geomodel by inserting a line implicitly defined. This avoids to globally rebuild the structural model and create a new mesh, from scratch, which takes time and effort (e.g., Pellerin et al., 2015; Zehner et al., 2015). Local editing techniques on geological models allow for small adjustments to the models without having to go through the entire mesh construction process. Although the principles are similar to those highlighted by Suter et al. (2017), we have proposed a strategy to maintain the mesh conformity, which is a prerequisite for many physical modeling codes. The implicit formulation is interesting for mesh simplifications and generalizations to more complex interfaces as long as they can be represented on the input mesh by a piecewise linear scalar field. This formulation allowed us to demonstrate the practical impact of model updating on wave propagation in a simple example of gas-water contact insertion into a cross-section. The simulation results permit to solve a Bayesian inverse problem, leading to a probabilistic estimation of the contact depth.

Some of the modified models have poor quality triangles, often located near the newly created corners. These triangles strongly impact the simulation time. In order to automate the reversal process, a quality threshold could be defined to automatically adjust the tolerance ϵ used in Section 3.3 and avoid excessively long simulations (Figure 18). Although this approach locally approximates the target geometry by projecting the level-set on nodes of the input mesh, it allows to automatically and robustly reduce mesh quality issues. As compared to the simplification methodology proposed by Anquez et al. (2019), this approach is more specific as it considers one interface at a time, but it is significantly easier to implement. So whereas the initial target of this work was not global model simplification as in the case of Anquez et al. (2019), we believe that a carefully designed incremental insertion of implicit interfaces could provide an alternative way to robustly address this problem by locally merging interfaces which are too close one from another. One may argue that such approximations should be avoided, but we consider that some of them are inevitable to obtain physical solutions in acceptable time. As discussed by Anquez et al. (2019), due to the limited resolution of the seismic wavefield, some mild interface modifications will only introduce negligible errors in the simulation results.

Coupling the local modifications with the evaluation of their impact by comparing to a reference model (by using wave propagation simulations), leads to the fact that the integration in an inversion code could be done in more complex settings (e.g., detecting fluid substitution during gas storage, CO_2 sequestration, or reducing the horizon position uncertainty (Bodin and Sambridge, 2009)).

More generally, the local insertion of an implicit interface into an existing mesh opens interesting perspectives to address other types of geological uncertainties, such as the simulations of undetected fractures and faults, or the management of stratigraphic uncertainties. As faults and fractures do not necessarily terminate against pre-existing boundaries, the definition of the region to be modified is essential. This particular region could be defined according to the object that we want to modify or insert. In two dimensions, this could be achieved by defining a circle centered on

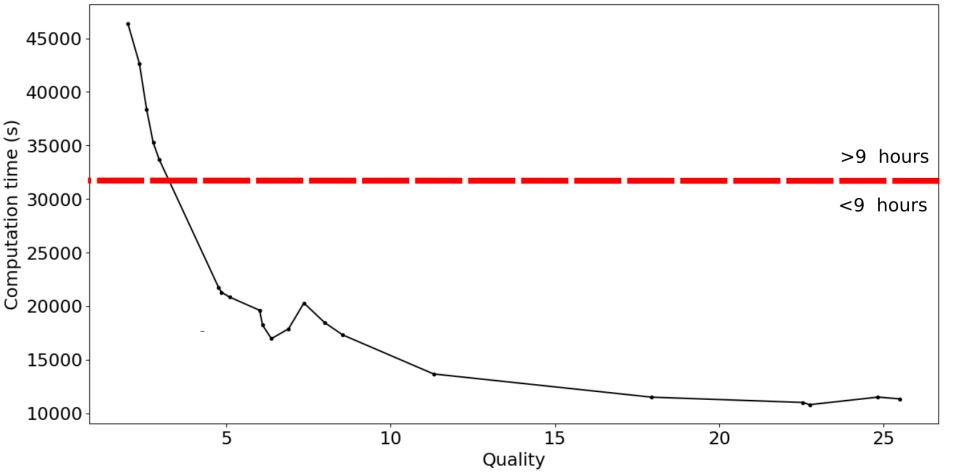

Figure 18: A quality threshold can be defined to avoid a high top simulation time. If the quality Q (2) is smaller than 3, the simulation time significantly increases (on a machine with a processor Intel(R) Xeon(R) CPU E5-1620 v2 @ 3.70GHz, 8 Cores).

the fracture to be inserted or more generally by a second level-set (Cherpeau et al., 2012; Moës et al., 2002). Finally, the zone to be remeshed could be defined by a number of rows of triangles around the fracture, so as to preserve the mesh quality during the insertion.

Although the principles discussed in this article for the local modification of a meshed geomodel in 2D could be extended in 3D, the transition from 2D to 3D geometric operations is seldom trivial. Indeed, the 2D geometric model editing operations are well understood and easily implemented, but the corresponding 3D operations often generate more complex configurations which are difficult to handle. Nonetheless, we are confident that the use of piecewise linear level-sets for local 3D mesh updating are very promising. As a matter of fact, it is already possible to discretize surfaces in 3D multi-material models using a similar workflow relying on the *mmg3d* code (Figure 19).

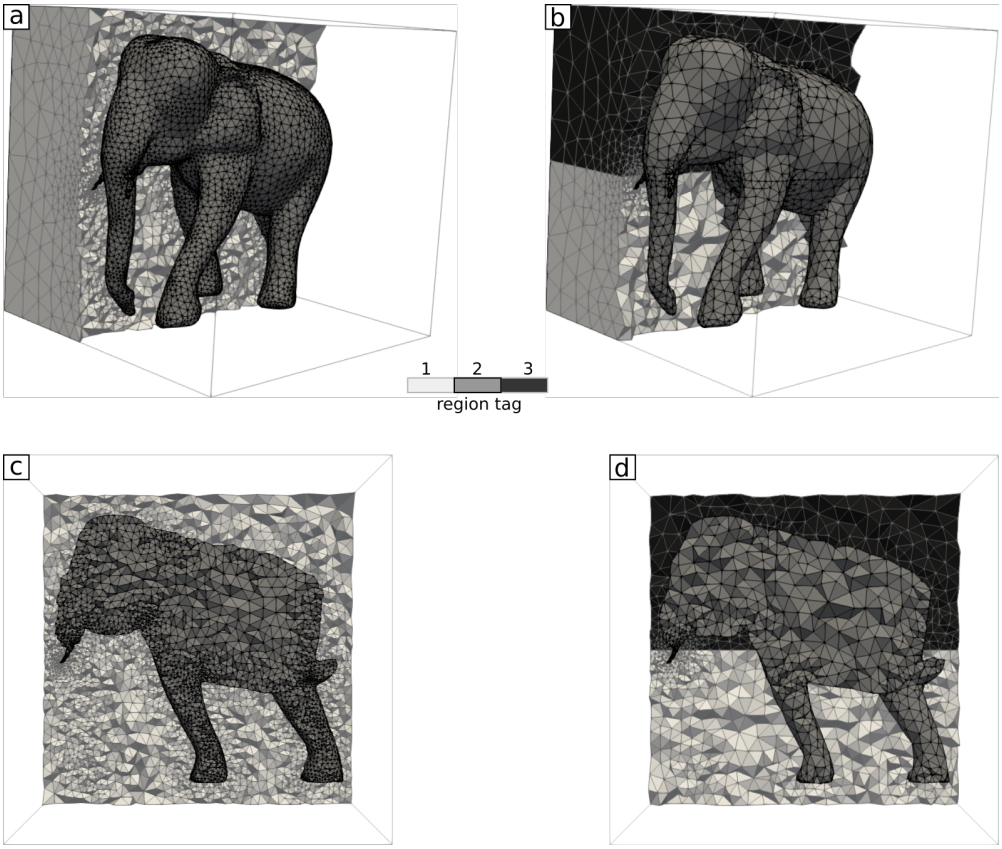

Figure 19: Insertion of an horizontal surface in multi-material model: (a, c) Initial multi material model; (b, d) The surface is inserted in the model only in the outer domain (1) of (a). The elephant is still composed of a unique region. The elephant surface is remeshed to maintain the conformity of the model.

Acknowledgments

This work was performed in the frame of the RING project (http://ring.georessources.univ-lorraine.fr) at Université de Lorraine. We would like to thank for their support the industrial and academic sponsors of the RING-GOCAD Consortium managed by ASGA. We also thank TOTAL for additional support for the PhD of Capucine Legentil. The software corresponding to this paper is available as a python and C++ code, which significantly relies on Mmg and Gmsh. We also acknowledge Inria and the Mmg Consortium for the hou10ni and Mmg libraries. The authors would also like to thank Hélène Barucq, Julien Diaz for their help.

Code availability section

Name of the code/library : LUMOS2D

Contact: capucine.legentil@univ-lorraine.fr

License: GNU GPL v.3

Hardware requirements: Linux System

Program language: Python

Software required: python 3.6 or 3.7, Mmg, Gmsh, shapely, VTK, meshio (to run the jupyter notebook)

Program size: 5Mo

The source codes are available for downloading at the link: https://github.com/ring-team/LUMOS2D

References

Abrahamsen, P., 1993. Bayesian kriging for seismic depth conversion of a multi-layer reservoir, in: Soares, A. (Ed.), Geostatistics Troia'92. Springer, pp. 385–398.

Allaire, G., Dapogny, C., Frey, P., 2014. Shape optimization with a level set based mesh evolution method. Computer Methods in Applied Mechanics and Engineering 282, 22–53.

Allaire, G., Jouve, F., Toader, A.M., 2004. Structural optimization using sensitivity analysis and a level-set method. Journal of Computational Physics 194, 363–393. doi:10.1016/j.jcp.2003.09.032.

Allen, R., Nilsen, H.M., Lie, K.A., Møyner, O., Andersen, O., 2018. Using simplified methods to explore the impact of parameter uncertainty on CO2 storage estimates with application to the Norwegian Continental Shelf. International Journal of Greenhouse Gas Control 75, 198–213. doi:10.1016/j.ijggc.2018.05.017.

Anquez, P., Pellerin, J., Irakarama, M., Cupillard, P., Lévy, B., Caumon, G., 2019. Automatic correction and simplification of geological maps and cross-sections for numerical simulations. Comptes Rendus Geoscience 351, 48–58. doi:10.1016/j.crte.2018.12.001.

Arts, R., Eiken, O., Chadwick, A., Zweigel, P., Vandermeer, L., Zinszner, B., 2003. Monitoring of CO2 Injected at Sleipner Using Time Lapse Seismic Data. Greenhouse Gas Control Technologies - 6th International Conference , 347–352doi:10.1016/b978-008044276-1/50056-8.

Barucq, H., 2016. Activity report magique 3d 2016. https://team.inria.fr/magique3d/research/software/hou10ni/.

Barucq, H., Djellouli, R., Estecahandy, E., 2014. Efficient DG-like formulation equipped with curved boundary edges for solving elasto-acoustic scattering problems. International Journal for Numerical Methods in Engineering 98, 747–780.

Benard, P., Balarac, G., Moureau, V., Dobrzynski, C., Lartigue, G., D'Angelo, Y., 2016. Mesh adaptation for large-eddy simulations in complex geometries. International Journal for Numerical Methods in Fluids 81, 719–740. doi:10.1002/fld.4204.

Bidmon, K., Rose, D., Ertl, T., 2004. Intuitive, Interactive, and Robust Modification and Optimization of Finite Element Models, in: Proceedings 13th International Meshing Roundtable., Albuquerque, NM, USA : Sandia National Laboratories. pp. 59–70.

Bodin, T., Sambridge, M., 2009. Seismic tomography with the reversible jump algorithm. Geophysical Journal International 178, 1411–1436. doi:10.1111/j.1365-246X.2009.04226.x.

Caumon, G., Gray, G., Antoine, C., Titeux, M.O., 2013. Three-dimensional implicit stratigraphic model building from remote sensing data on tetrahedral meshes: Theory and application to a regional model of la Popa Basin, NE Mexico. IEEE Transactions on Geoscience and Remote Sensing 51, 1613–1621. doi:10.1109/TGRS.2012.2207727.

Caumon, G., Sword, C.H., Mallet, J.L., 2003. Constrained modifications of non-manifold B-reps, in: Proceedings of the eighth ACM symposium on Solid modeling and applications - SM '03, ACM Press, New York, New York, USA. p. 310. doi:10.1145/781650.781657.

Cherpeau, N., Caumon, G., Caers, J., Lévy, B., 2012. Method for Stochastic Inverse Modeling of Fault Geometry and Connectivity Using Flow Data. Mathematical Geosciences 44, 147–168. doi:10.1007/s11004-012-9389-2.

Chilès, J.P., Aug, C., Guillen, A., Lees, T., 2004. Modelling the geometry of geological units and its uncertainty in 3d from structural data: the potential-field method, in: R. Dimitrakopoulos, S. Ramazan (eds.), Proceedings of international symposium on orebody modelling and strategic mine planning, Perth, Australia, pp. 313–320.

Collon, P., Caumon, G., 2017. 3D geomodelling in structurally complex areas - Implicit vs. explicit representations, in: 79th EAGE Conference and Exhibition 2017. doi:10.3997/2214-4609.201701144.

Dapogny, C., Dobrzynski, C., Frey, P., 2014. Three-dimensional adaptive domain remeshing, implicit domain meshing, and applications to free and moving boundary problems. Journal of Computational Physics 262, 358–378. doi:10.1016/j.jcp.2014.01.005.

Dobrzynski, C., Frey, P., 2008. Anisotropic delaunay mesh adaptation for unsteady simulations. Proceedings of the 17th International Meshing Roundtable, IMR 2008 , 177–194doi:10.1007/978-3-540-87921-3_11.

Durand-Riard, P., Caumon, G., Muron, P., 2010. Balanced restoration of geological volumes with relaxed meshing constraints. Computers & Geosciences 36, 441–452. doi:10.1016/j.cageo.2009.07.007.

Euler, N., Sword Jr, C.H., Dulac, J.C., 1999. Editing and rapidly updating a 3d earth model, in: SEG Technical Program Expanded Abstracts 1999. Society of Exploration Geophysicists, pp. 950–953.

Geller, R.J., Takeuchi, N., 1995. A new method for computing highly accurate DSM synthetic seismograms. Geophysical Journal International 123, 449–470.

Geuzaine, C., Remacle, J.F., 2009. Gmsh: A 3-D finite element mesh generator with built-in pre- and post-processing facilities. International Journal for Numerical Methods in Engineering 79, 1309–1331. doi:10.1002/nme.2579.

Giraud, J., Lindsay, M., Jessell, M., 2021. Generalization of level-set inversion to an arbitrary number of geological units in a regularized least-squares framework. Geophysics , 1–76doi:10.1190/geo2020-0263.1.

Grote, M.J., Schneebeli, A., Schötzau, D., 2006. Discontinuous Galerkin finite element method for the wave equation. SIAM Journal on Numerical Analysis 44, 2408–2431.

Guillén, A., Sovilj, D., Lendasse, A., Mateo, F., Rojas, I., 2008. Minimising the delta test for variable selection in regression problems. International Journal of High Performance Systems Architecture 1, 269–281. doi:10.1504/IJHPSA.2008.024211.

Guo, Z., de Hoop, M.V., 2013. Shape optimization and level set method in full waveform inversion with 3D body reconstruction, in: SEG Technical Program Expanded Abstracts 2013, Society of Exploration Geophysicists. pp. 1079–1083. doi:10.1190/segam2013-1057.1.

Guttman, A., 1984. R-trees: a dynamic index structure for spatial searching, in: Proceedings of the 1984 ACM SIGMOD international conference on Management of data - SIGMOD '84, ACM Press, New York, New York, USA. p. 47. doi:10.1145/602259.602266.

Hamada, G., 2004. Reservoir fluids identification using vp/vs ratio? Oil & Gas Science and Technology 59, 649–654.

Houlding, S.W., 1994. 3D Geoscience Modeling. Springer Berlin Heidelberg, Berlin, Heidelberg. doi:10.1007/978-3-642-79012-6.

Jacquet, P., 2021. FWI (Full Waveform Inversion) dans le domaine temporel utilisant des méthodes numériques hybrides pour la caractérisation de milieux élasto-acoustiques. Ph.D. thesis.

Landrø, M., Veire, H.H., Duffaut, K., Najjar, N., 2003. Discrimination between pressure and fluid saturation changes from marine multicomponent time-lapse seismic data. Geophysics 68, 1592–1599. doi:10.1190/1.1444973.

Laurent, G., Caumon, G., Jessell, M., 2015. Interactive editing of 3D geological structures and tectonic history sketching via a rigid element method. Computers & Geosciences 74, 71–86. doi:10.1016/j.cageo.2014.10.011.

Ledez, D., 2003. Modélisation d'objets naturels par formulation implicite. Ph.D. thesis. Institut National Polytechnique de Lorraine.

Lévy, B., 2016. Robustness and efficiency of geometric programs: The Predicate Construction Kit (PCK). CAD Computer Aided Design 72, 3–12. doi:10.1016/j.cad.2015.10.004.

Li, C., Pion, S., Yap, C., 2005. Recent progress in exact geometric computation. The Journal of Logic and Algebraic Programming 64, 85–111. doi:10.1016/j.jlap.2004.07.006.

Loseille, A., Dervieux, A., Alauzet, F., 2010. Fully anisotropic goal-oriented mesh adaptation for 3D steady Euler equations. Journal of Computational Physics 229, 2866–2897. doi:10.1016/j.jcp.2009.12.021.

MacKay, D.J., 2003. Information theory, inference and learning algorithms. Cambridge university press.

Mallet, J.L., 1988. Three-dimensional graphic display of disconnected bodies. Mathematical Geology 20, 977–990. doi:10.1007/BF00892974.

Mallet, J.L., 2004. Geomodeling. Oxford University Press. doi:10.1023/b:matg.0000020673.98166.ea.

Mari, J., Yven, B., 2014. The application of high-resolution 3D seismic data to model the distribution of mechanical and hydrogeological properties of a potential host rock for the deep storage of radioactive waste in France. Marine and Petroleum Geology 53, 133–153. doi:10.1016/j.marpetgeo.2013.10.014.

Moës, N., Gravouil, A., Belytschko, T., 2002. Non-planar 3D crack growth by the extended finite element and level sets-Part I: Mechanical model. International Journal for Numerical Methods in Engineering 53, 2549–2568. doi:10.1002/nme.429.

Mulrooney, M.J., Osmond, J.L., Skurtveit, E., Faleide, J.I., Braathen, A., 2020. Structural analysis of the Smeaheia fault block, a potential CO2 storage site, northern Horda Platform, North Sea. Marine and Petroleum Geology 121, 104598. doi:10.1016/j.marpetgeo.2020.104598.

Osher, S.J., Santosa, F., 2001. Level Set Methods for Optimization Problems Involving Geometry and Constraints I. Frequencies of a Two-Density Inhomogeneous Drum. Journal of Computational Physics 171, 272–288. doi:10.1006/jcph.2001.6789.

Pellerin, J., Botella, A., Bonneau, F., Mazuyer, A., Chauvin, B., Lévy, B., Caumon, G., 2017. RINGMesh: A programming library for developing mesh-based geomodeling applications. Computers & Geosciences 104, 93–100. doi:10.1016/j.cageo.2017.03.005.

Pellerin, J., Caumon, G., Julio, C., Mejia-Herrera, P., Botella, A., 2015. Elements for measuring the complexity of 3d structural models: Connectivity and geometry. Computers & Geosciences 76, 130–140.

Reed, W.H., Hill, T.R., 1973. Triangular mesh methods for the neutron transport equation. Technical Report. Los Alamos Scientific Lab., N. Mex.(USA).

Ringrose, P., Bentley, M., 2015. Reservoir Model Design. Springer Netherlands, Dordrecht. doi:10.1007/978-94-007-5497-3.

Riviere, B., 2008. Discontinuous Galerkin methods for solving elliptic and parabolic equations: theory and implementation. SIAM.

Santosa, F., 1996. A level-set approach for inverse problems involving obstacles. ESAIM - Control, Optimisation and Calculus of Variations 1, 17–33. doi:10.1051/cocv:1996101.

Sethian, J., Wiegmann, A., 2000. Structural Boundary Design via Level Set and Immersed Interface Methods. Journal of Computational Physics 163, 489–528. doi:10.1006/jcph.2000.6581.

Shaw, J.H., Plesch, A., Tape, C., Suess, M.P., Jordan, T.H., Ely, G., Hauksson, E., Tromp, J., Tanimoto, T., Graves, R., Olsen, K., Nicholson, C., Maechling, P.J., Rivero, C., Lovely, P., Brankman, C.M., Munster, J., 2015. Unified Structural Representation of the southern California crust and upper mantle. Earth and Planetary Science Letters 415, 1–15. doi:10.1016/j.epsl.2015.01.016.

Shewchuk, J.R., 1997. Adaptive precision floating-point arithmetic and fast robust geometric predicates. Discrete and Computational Geometry 18, 305–363. doi:10.1007/pl00009321.

Si, H., 2015. TetGen, a delaunay-based quality tetrahedral mesh generator. ACM Transactions on Mathematical Software 41. doi:10.1145/2629697.

Suter, E., Cayeux, E., Friis, H.A., Kårstad, T., Escalona, A., Vefring, E., 2017. A Novel Method for Locally Updating an Earth Model While Geosteering. International Journal of Geosciences 08, 237–264. doi:10.4236/ijg.2017.82010.

Sword Jr, C.H., 1991. Building flexible interactive geologic models, in: SEG Technical Program Expanded Abstracts 1991. Society of Exploration Geophysicists, pp. 1465–1467.

Tertois, A.L., Mallet, J.L., 2007. Editing faults within tetrahedral volume models in real time. Geological Society Special Publication 292, 89–101. doi:10.1144/SP292.5.

Wang, M.Y., Chen, S., Wang, X., Mei, Y., 2005. Design of Multimaterial Compliant Mechanisms Using Level-Set Methods. Journal of Mechanical Design 127, 941–956. doi:10.1115/1.1909206.

Wang, M.Y., Wang, X., Guo, D., 2003. A level set method for structural topology optimization. Computer Methods in Applied Mechanics and Engineering 192, 227–246. doi:10.1016/S0045-7825(02)00559-5.

Wang, Y., Luo, Z., Kang, Z., Zhang, N., 2015. A multi-material level set-based topology and shape optimization method. Computer Methods in Applied Mechanics and Engineering 283, 1570–1586. doi:10.1016/j.cma.2014.11.002.

Wellmann, F., Caumon, G., 2018. 3-d structural geological models: Concepts, methods, and uncertainties, in: Advances in Geophysics. Elsevier. volume 59, pp. 1–121.

Zehner, B., Börner, J.H., Görz, I., Spitzer, K., 2015. Workflows for generating tetrahedral meshes for finite element simulations on complex geological structures. Computers & Geosciences 79, 105–117.

Zheglova, P., Lelièvre, P.G., Farquharson, C.G., 2018. Multiple level-set joint inversion of traveltime and gravity data with application to ore delineation: A synthetic study. Geophysics 83, R13–R30. doi:10.1190/geo2016-0675.1.